Electronic Journal of University of Aden for Basic and Applied Sciences
EJUA-BA Vol. 4 No. 3 (2023)
https://doi.org/10.47372/ejua-ba.2023.3.273
ISSN: 2708-0684

RESEARCH ARTICLE

THE STRUCTURAL AND ELECTRICAL PROPERTIES OF NON-STOICHIOMETRIC CADMIUM SELENIDE THIN FILMS

Abdullah Omar Ali[1,*], Mehdi A. Dabban[1], and H. Mahfoz Kotb[2]

[1] *Physics Department, Faculty of Science, University of Aden, Yemen*
[2] *Physics Department, Faculty of Education, Assiut University, Egypt*

***Corresponding author: Abdullah Omar Ali; E-mail: abdullah.omer.scie@aden-univ.net**

Received: 02 August 2023 / Accepted: 16 August 2023 / Published online: 30 September 2023

Abstract

Non-stoichiometric Cd_xSe_{100-x} (x=10, 20, 30 at. %) alloys were prepared by melt-quenching technique, while thin films of these alloys were prepared by vacuum thermal evaporation technique. The Differential thermal analysis (DTA) results showed that the composition affects the characteristic temperatures, for instance, the glass transition, and peak crystallization temperatures. X-ray diffraction patterns (XRD) of the as-deposited films confirmed its amorphous nature except for films with x=30 at. %. These results were confirmed by scanning electron microscopy (SEM) investigations and correlated to the rigidity percolation threshold of the lattice. Furthermore, XRD patterns indicated that amorphous structures transformed into crystalline structures for annealed thin films at 423 K for 30 minutes. The microstructure parameters (crystal size, microstrain, and dislocation density) of both Se and CdSe phases were calculated for annealed films. The temperature dependence of dark d.c. conductivity of thin films was studied in the temperature range (300-500 K). The electrical measurements results showed two types of conduction mechanisms. Conduction is due to extended state in the temperature range (370-500 K) and variable range hopping in the temperature range (300-370 K). Moreover, in the high temperature range, the results indicate the validity of Meyer-Neldel rule (MNR) in the studied samples.

Keywords: Cadmium selenide, Thin films, Rigidity percolation threshold, Dark d.c. conductivity, Meyer-Neldel rule.

1. Introduction

Among the II-IV compounds, Cadmium Selenide system [1] is a promising semiconductor material for fabrication of heterojunction solar cells, laser and photoelectrochemical cells, light emitting diodes, and photodetectors [2, 3]. Because of their suitable bandgap (1.7 eV in bulk form) and high photosensitivity in the visible range of the solar spectrum, these materials can be advantageously used for low cost applications. Different physical and chemical techniques are available for the growth of CdSe thin films [4, 5]. Several workers [6, 7] have reported the effect of growth conditions and thermal treatments on the structural, optical, and electrical properties of CdSe thin films for use in device fabrication. Nevertheless, little attention has been given to the effect of composition on the properties of thermally evaporated non-stoichiometric Cd_xSe_{100-x} thin films [8, 9]. Moreover, these studies have dealt only with the optical properties of the as-prepared Cd_xSe_{100-x} (x: 30-60 %) thin films.

Previously [10, 11], we studied the effect of annealing on the structural, electrical and optical properties of amorphous selenium rich $Cd_{10}Se_{90}$ thin films (SR-CdSe). The annealed films of SR-CdSe exhibited a polycrystalline nature with Se phase in the major proportion as compared to the CdSe phase with both phases exhibit a hexagonal structure. In the present work, these investigations are extended by studying the structural changes due to Cd content for the as-prepared and annealed Cd_xSe_{100-x} (x=10, 20, 30 at. %) films. Besides, the dependence of the electrical properties of these films on the Cd content was studied in the temperature range (300-500 K) to understand the conduction mechanism tacking place in this important semiconductor material.

2. Experimental procedures

The bulk samples of Cd_xSe_{100-x} (x=10, 20, 30 at. %) were prepared from a mixture of Cd and Se elements with purity 99.999% (Aldrich Chem Co,USA). The constituent elements were weighed according to their atomic percentage and were sealed in a quartz ampoule (inner diameter ~ 8 mm) under vacuum of 10^{-5} Torr. The sealed ampoules were kept inside a furnace and heated up gradually to 873 K. The constituents hereafter were kept at 1173 K for 16h. Continuous stirring of the melt was carried out to ensure good homogeneity. The melt was then rapidly quenched in ice-water mixture. After quenching, the solid ingots were removed from the ampoules and kept in dry atmosphere. Differential thermal analyzer (DTA) measurements were carried out on the as-prepared fine powder samples by using Shimadzu DTA-50 under non-isothermal conditions in N_2 atmosphere at 5 K/min heating rate.

Thin films of cadmium selenide were deposited onto chemically-cleaned glass substrates kept at room temperature by thermal evaporation technique using a high vacuum coating unit (E306A, Edwards Co., UK). During the deposition process (at normal incidence), the substrates were suitably rotated in order to obtain films of uniform thickness. The thickness of the films (~ 600 nm) was measured by a mechanical profilometer (KLA Tencor P.15). Annealing of the films was carried out in Pyrex tube furnace at 423 K for 30 min under flow of pure nitrogen.

The phase structure of the films was examined by using X-ray diffractometer (Philips type PW 1710 with Cu as a target and Ni as a filter, λ=1.5418 Å). The morphology of the as-prepared as well as the annealed films was examined using scanning electron microscope (SEM), Jeol (JSM)-T200 type. The chemical composition of the as-prepared films was measured using the standard Energy Dispersive analysis of X-ray (EDX) unit attached to the used electron microscope. Thick aluminum electrodes were thermally deposited as ohmic contact. A planar geometry of the amorphous films (electrode gap ~ 2 mm) was used for the electrical measurements. Keithley 610 C electrometer was used as ohmmeter. The temperature was measured using a calibrated copper constantan thermocouple. The temperature dependence of d.c. conductivity of the Cd_xSe_{100-x} (x=10, 20, 30 at.%) films was then measured under dark conditions in the temperature range 300-475 K.

3. Theoretical Background

The average coordination numbers 〈N〉 of the studied glasses were evaluated [12] using the following equation and the values of 〈N〉 are given in Table 3.

$$\langle N\rangle = \left(xN^{Cd} + (100-x)N^{Se}\right)/100 \qquad (1)$$

where N^{Cd} and N^{Se} represent the coordination number of Cd and Se elements which are 4 and 2, respectively [13].

The deviation of stoichiometry S is expressed by the ratio of covalent bonding possibilities of chalcogen atom to that of non-chalcogen atom. Values of S were found to be larger than unity for chalcogen-rich glasses and less than unity for chalcogen-poor glasses. The values of S were calculated using the following relation [14]:

$$S = \frac{(100-x)N^{Se}}{xN^{Cd}} \qquad (2)$$

The calculated values of S were found to be 4.5, 2 and 1.17 for $Cd_{10}Se_{90}$, $Cd_{20}Se_{80}$ and $Cd_{30}Se_{70}$, respectively which indicates chalcogen-rich compositions.

Heteronuclear single bond energies E_{A-B} can be related to the homonuclear bonds E_{A-A} and E_{B-B} by Pauling's relation [15]:

$$E_{A-B} = \left[E_{A-A}.E_{B-B}\right]^{1/2} + a(\chi_A - \chi_B)^2 \qquad (3)$$

where E(A-B) is the bond energy of heteronuclear bond; E(A-A) and E(B-B) are energies of expected homonuclear bonds (3.425 eV and 0.076 eV for Se and Cd, respectively) [16]; χ_A and χ_B are the electronegativity values for the involved atoms (2.55 and 1.69 for Se and Cd, respectively) [16].

According to Tichy and Ticha [17], the value of glass transition temperature should not be only related to connectedness of the network (which is related to 〈N〉) but should also be related to the quality of connections, i.e. the mean bond energy between the atoms of the network. Since the difference in the bond energies of heteronuclear and homonuclear bonds is substantial, so chemically ordered network are expected where the number of heteronuclear bonds is maximized i.e. they are more favorably formed than homonuclear bonds. Based on this assumption the over all mean bond energy 〈E〉 is given by [18]:

$$\langle E\rangle = E_c + E_{rm} \qquad (4)$$

where E_c is the mean bond energy of average cross-linking per atoms i.e, the overall contribution towards bond energy arising from strong heteronuclear bonds [19] are given as:

$$E_c = P_{rich}P_{hb}, \quad r>1 \text{ (chalcogen-rich)} \qquad (5\text{-a})$$

or

$$E_c = P_{poor}P_{hb}, \quad r<1 \text{ (chalcogen-poor)} \qquad (5\text{-b})$$

where P_{rich} and P_{poor} represent the degree of cross-linking per atoms for chalcogen-rich case and the chalcogen-poor one, respectively and are given by:

$$P_{rich} = xN^{A}/(x+y) \quad (6\text{-a})$$

$$P_{poor} = yN^{B}/(x+y) \quad (6\text{-b})$$

The average heteronuclear bond energy E_{hb} is given by:

$$E_{hb} = \frac{xN^{A}E_{A-B}}{xN^{A}} \quad (7)$$

where E_{A-B} is the heteronuclear bond energy of the A-B heteronuclear bonds. The second term in Eq. (4), E_{rm}, is the average bond energy per atom of the remaining matrix i.e. the contribution arising from weaker bonds that remain after the strong bonds have been maximized [19], which is defined as

$$\langle E_{rm} \rangle = \frac{2[0.5\langle N\rangle - P_{rich}]E_{B-B}}{\langle N\rangle}, \text{ for } S>1 \quad (8\text{-a})$$

$$\langle E_{rm} \rangle = \frac{2[0.5\langle N\rangle - P_{poor}]E_{A-A}}{\langle N\rangle}, \text{ for } S<1 \quad (8\text{-b})$$

In Eq. (8), E_{B-B} is the homounclear bond energy of Se-Se bonds and E_{A-A} is the average bond energy of a "metal-metal" bond in the chalogen-poor region.

4. Results and discussion

4.1 Structural analysis

The quantitative analysis of Cd_xSe_{100-x} (x=10, 20, 30 at. %) films were carried out using EDX technique. The elemental analysis was carried out the presence of Cd, and Se. The constituent element ratio of the investigated thin films were 9.92: 90.08, 20.65: 79.35 and 32.95: 67.05 for $Cd_{10}Se_{90}$, $Cd_{20}Se_{80}$ and $Cd_{30}Se_{70}$ samples, respectively, which is near to the nominal compositions. **Fig. 1**$_{a,b,c}$ shows the spectral distribution of the constituent elements for the Cd_xSe_{100-x} (x = 10, 20 and 30 at. %) thin films.

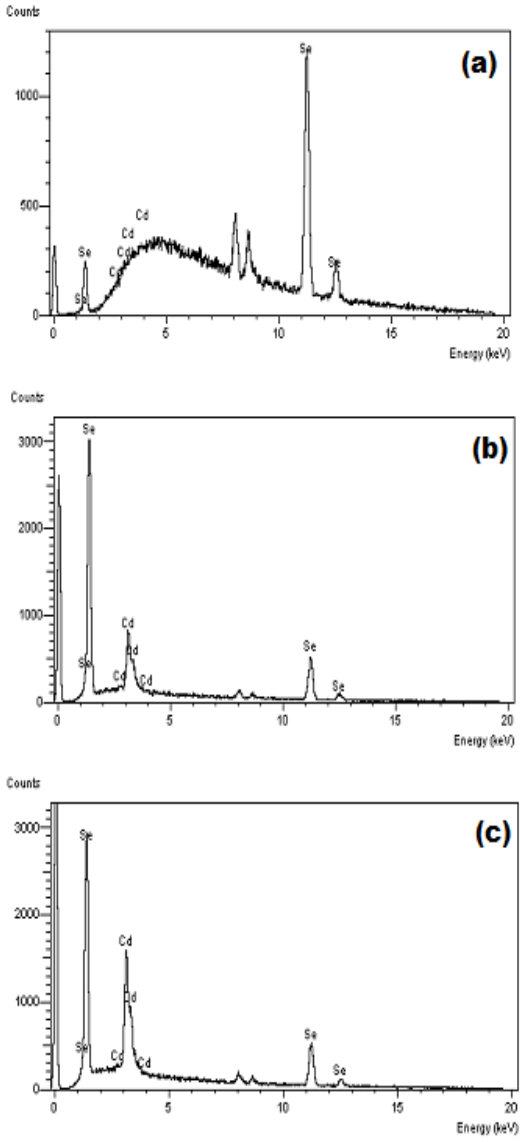

Fig. (1): Energy dispersive spectral distribution of the constituent elements for (a) $Cd_{10}Se_{90}$, (b) $Cd_{20}Se_{80}$ and (c) $Cd_{30}Se_{70}$ thin films.

A typical DTA traces for the as prepared powder samples of Cd_xSe_{100-x} (x=10, 20, 30 at %) at a 5 K/min heating rate in the temperature range (300-550 K) are shown in **Fig.2**. It can be seen from this figure that all the Cd_xSe_{100-x} glasses show one glass transition and one stage crystallization on heating. The characteristic temperatures namely glass transition (T_g), the onset crystallization (T_c), the peak of crystallization (T_p) and the melting (T_m) temperatures determined from the DTA scans are listed in **Table 1**. It is noticed that with

increasing Cd content, both T_c and T_p increases, while T_g decreases. The glass transition temperature is known to depend on the overall bond energy 〈E〉 [20]. The decrease in T_g with increasing Cd content is consistent with the decrease in the overall bond energy 〈E〉 for our samples as shown in **Table 1**.

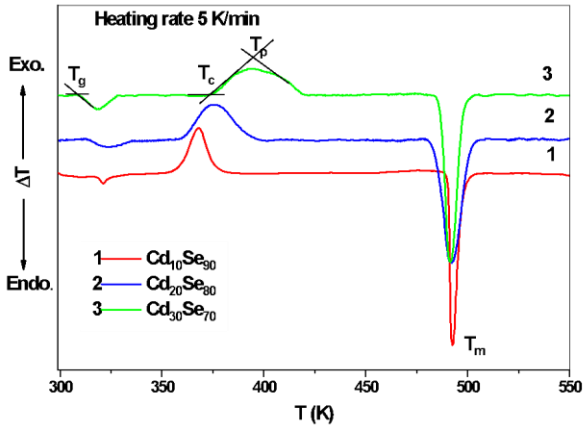

Fig. (2): DTA traces for Cd_xSe_{100-x} (x=10, 20, 30 at. %) at heating rate 5 K/min.

Table 1: The average coordination number, <N>, the number of constraints, N_{cons}, the deviation of stoichiometry, r, the overall mean bond energy <E> and the thermal parameters T_g, T_c, T_p, and T_m for Cd_xSe_{100-x} (x=10, 20, 30 at. %).

Composition	〈N〉	S	T_g (K)	T_c (K)	T_p (K)	T_m(K)	〈E〉 eV	N_{con}
$Cd_{10}Se_{90}$	2.2	4.5	318	353	368	487	2.768	2.5
$Cd_{20}Se_{80}$	2.4	2	314	358.9	375	480	2.319	3
$Cd_{30}Se_{70}$	2.6	1.17	309	373	394	483	2.029	3.5

Fig. $3_{a,b}$ show the XRD patterns of the as-prepared and annealed Cd_xSe_{100-x} (x=10, 20, 30 at.%) thin films, respectively. The as-prepared samples with x=10 and 20 at.% are amorphous while the sample with x=30 at.% is poor crystalline where one crystalline peak appeared at 2θ = 23.2° (d=3.834) embedded in a hump representing an amorphous matrix. This peak was indexed according to JCPDS file no. (75-1162) of monoclinic Se.

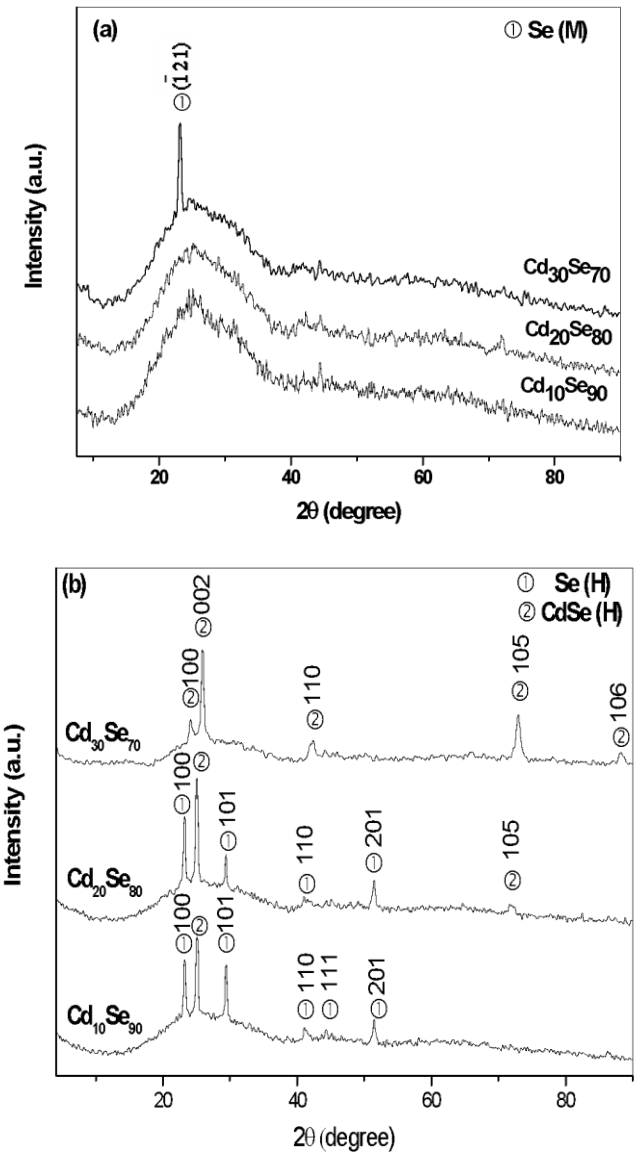

Fig. (3): X-ray diffraction patterns of Cd_xSe_{100-x} (x=10, 20, 30 at %) films: (a) as-prepared; (b) annealed at 423 K for 30 min in N_2 atmosphere.

The XRD patterns of annealed Cd_xSe_{100-x} (x=10, 20, 30 at.%) thin films at 423 K for 30 min in N_2 atmosphere, revealed the polycrystalline nature of these films. Analyzing XRD patterns reveals the coexistence of both Se and CdSe crystalline phases according to JCPDS files (Hexagonal CdSe no. 02–0330, Hexagonal CdSe no. 04-011-9600 and Hexagonal Se no. 86–2246, Hexagonal Se no. 04-002-2932). The interplanar spacing (d) for orientation peaks of both Se and CdSe crystalline phases was calculated using Bragg's formula ($d=\lambda/2\sin\theta$) where θ is the Bragg's angle, λ is the wavelength of the used X-ray. The lattice parameters (c) for annealed films were calculated for hexagonal structure by the equation [20]:

$$\frac{1}{d_{hkl}^2} = \frac{4}{3}\left[\frac{h^2+hk+k^2}{a^2}\right] + \frac{l^2}{c^2} \qquad (9)$$

where h, k, and l represent the lattice planes. From **Table 2**, we note that the calculated values for the parameters d and c for annealed thin films are in a good agreement with the standard JCPDS data files for Se and CdSe hexagonal phases. Formation of the hexagonal phase is perhaps due to the non-stoichiometric ratio of Cd and Se in the films [21].

The crystallite size for annealed films is calculated using the Scherrer formula from the full width at half maximum (FWHM), β [22].

$$D = \frac{0.94\lambda}{\beta\cos\theta} \qquad (10)$$

were D is the average diameter of crystallites, θ is Bragg's angle, β is the FWMH in radian and λ=1.5418 Å for the CuK_α radiation. Residual strain (ε) of annealed CdSe films are calculated from the following relation [23, 24]:

$$\varepsilon = \left[\frac{\lambda}{D\cos\theta} - \beta\right]\frac{1}{\tan\theta} \qquad (11)$$

The dislocation density (δ), defined as the length of dislocation lines per unit volume, is evaluated using the relation [25]:

$$\delta = \frac{1}{D^2} \qquad (12)$$

where D is the crystallite size. The calculated values of crystallite size, strain and dislocation density of the annealed thin films are included in Table 2. The increase in crystallite size values for the annealed samples from 28.07 nm to 48.9 nm in Se phase and from 30.79 nm to 89.49 nm in CdSe phase shows the improvement in the crystallinity of the films. Similar trend of increase in crystallite size and decrease in strain with increase of Cd content is observed for vacuum evaporated CdSe films on glass substrates [11]. Since the dislocation density and strain are manifestation of dislocation network in the films, the decrease in the strain and dislocation density indicates the formation of high quality films at higher Cd content.

Table 2: The structural parameters of the annealed Cd_xSe_{100-x} (x=10, 20 and 30%) thin films at 423 K for 30 min in N_2 atmosphere..

Composition	Phase	2θ Degree	h k ℓ	Lattice spacing, d (Å)		Lattice parameters, c (Å)		Crystallite Size, D, (nm)	Strain, ε×10-3	Dislocation density, δ×1015 (m-2)	No. of crystallites N×1016 (m2)
				Observed	Standard	Observed	Standard				
Cd10Se90	CdSe (H)	25.06	0 0 2	3.553	3.520	7.106	7.020	28.07	1.30	1.26	2.712
	Se (H)	29.38	1 0 1	3.072	3.007	4.998	4.958	30.79	1.39	1.05	2.055
Cd20Se80	CdSe (H)	25.01	0 0 2	3.56	3.520	7.120	7.020	48.90	0.75	0.42	0.513
	Se (H)	29.38	1 0 1	3.043	3.007	5.016	4.958	69.83	0.62	0.21	0.176
Cd30Se70	CdSe (H)	25.91	0 0 2	3.439	3.473	6.878	6.946	89.49	0.46	0.124	0.084

For more understanding of this behavior for Cd_xSe_{100-x} (x=10, 20, 30 at. %), the constraints theory proposed by Philips and Thorpe [26] was applied. In a covalently bonded glassy network two types of constraints should be considered: bond-stretching (α) and bond-bending (β) [27]. Given the average coordination number of the network $\langle N\rangle$, both α and β can be easily calculated from $\langle N\rangle$: $\alpha = \langle N\rangle/2$ and $\beta = 2\langle N\rangle - 3$. Thus the total number of constraints N_{con} can be expressed as:

$$N_{con} = \left[\frac{5}{2}\langle N\rangle - 3\right] \qquad (13)$$

The calculated values of N_{con} of Cd_xSe_{100-x} system are listed in **Table 1**. According to the constraints theory, the value $\langle N\rangle = 2.4$ is known as the rigidity percolation threshold (RPT). At $\langle N\rangle = 2.4$, the number of constraints N_{con} acting on the network are balanced by the degree of freedom N_d available for the atoms in the network, the structure becomes just rigid, and stable glasses can be prepared. In a glass with $\langle N\rangle$ lower than 2.4, the structure is floppy. Above this value, the structure is over constrained, and glass formation becomes difficult. It can be seen from **Table 1** that N_{con} increases with increasing Cd content and that an amorphous to crystalline transformation takes place at $\langle N\rangle = 2.6$ which corresponds to $Cd_{30}Se_{70}$ which is consistent with the constraints theory.

SEM micrographs of **Fig. 4**$_{a,b}$ show the surface morphology of the as-prepared $Cd_{20}Se_{80}$ and $Cd_{30}Se_{70}$ thin films. While the sample $Cd_{20}Se_{80}$ shows a completely amorphous matrix without any distinguishable agglomerations, the sample $Cd_{30}Se_{70}$ shows some small crystallites in the amorphous matrix. Comparing the SEM and XRD results suggests that these small crystallites might be monoclinic Se phase. On the other hand, the surface morphology of the films annealed

at 423 K for 30 min in N_2 atmosphere shows small crystallite that are uniformly distributed over amorphous homogenous background for x=10 at.% (**Fig.5$_a$**). Increasing the Cd content in films (x= 20, and 30 at. %) leads to increase the size and the faction content of the CdSe phase as shown in (**Fig.5$_{b,c}$**). Comparing again the SEM and XRD results of the annealed films then suggests that the large crystallites in this case might be principally the CdSe phase.

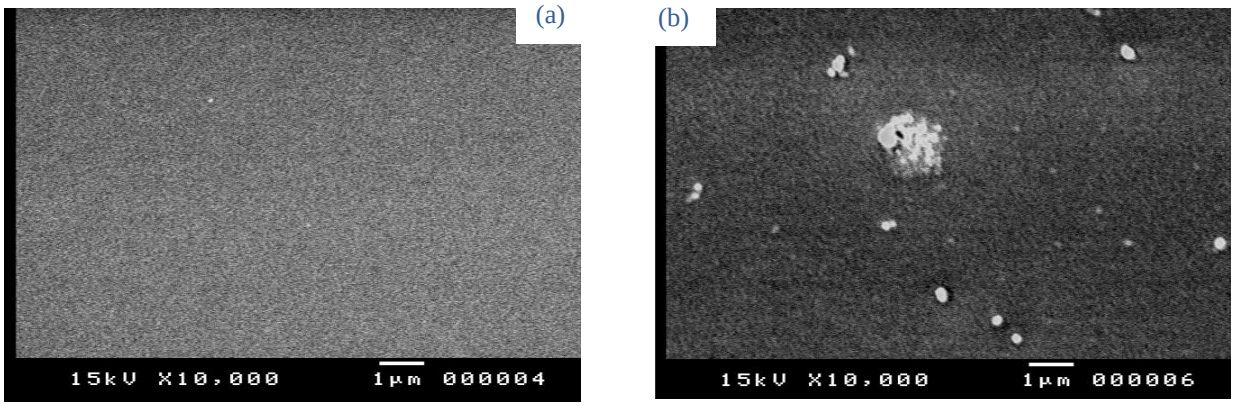

Fig. (4): SEM photograph of the as-prepared (a) $Cd_{20}Se_{80}$ and (b) $Cd_{30}Se_{70}$ thin films.

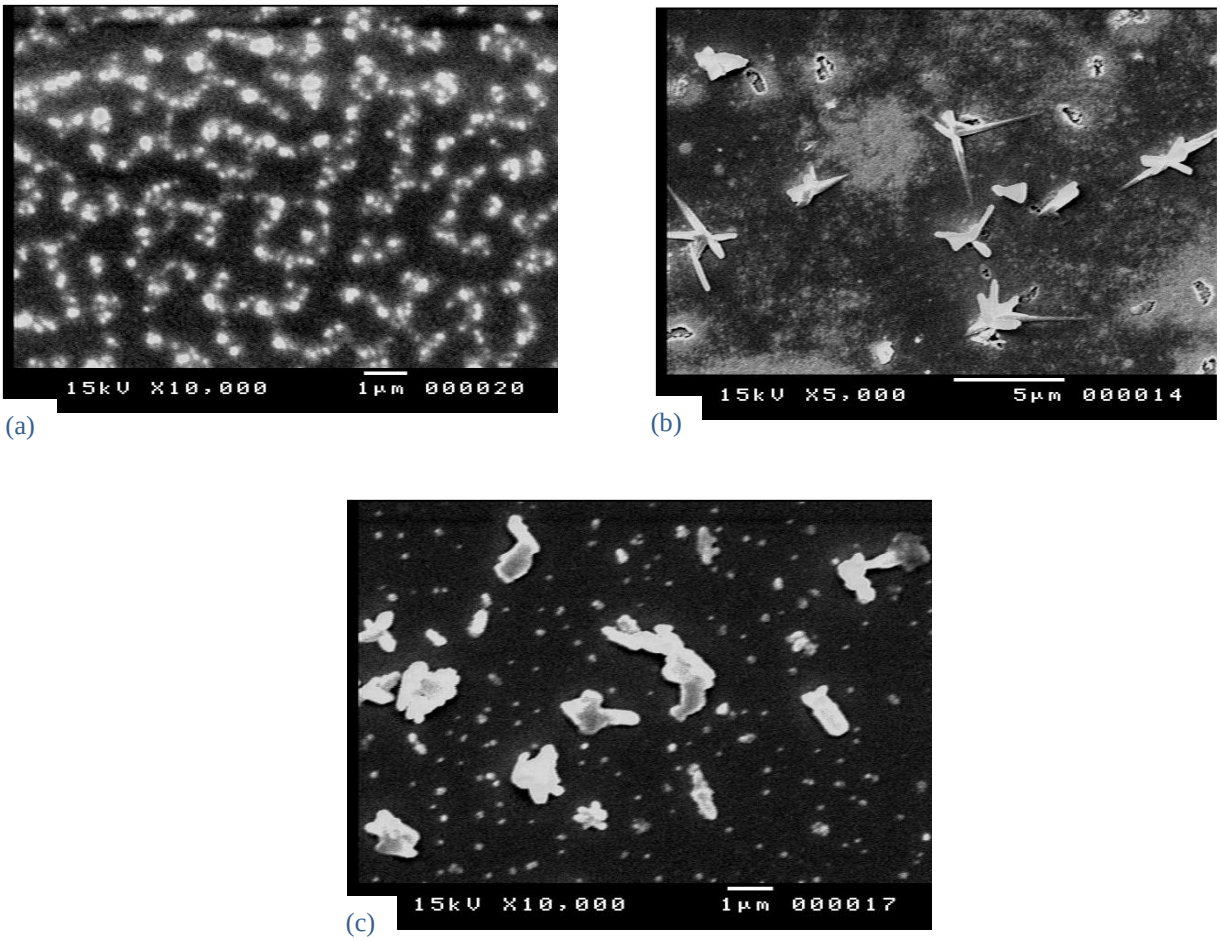

Fig. (5): SEM photograph of annealed at 423 K for 30 min in N_2 atmosphere: (a) $Cd_{10}Se_{90}$, (b) $Cd_{20}Se_{80}$ and (c) $Cd_{30}Se_{70}$ thin films.

4.2 Effect of Cd content on the transport mechanism

The d.c. conductivity as a function of the reciprocal temperature in the temperature range 300-500 K for Cd_xSe_{100-x} thin films is given in **Fig. 6**. This range of temperature was chosen to include both T_g and T_c of these alloys. Thus the effect of amorphous-to-crystalline phase transformation on the electrical properties can be investigated. It is clear from this **Fig. 6** that at any given temperature the d.c. conductivity increases with increasing Cd content which may be attributed to the higher electrical conductivity of the Cd compared to that of Se. Besides, all the samples showed the same behavior where the conductivity curve is made up of two linear regions indicating an activated process having two different conduction mechanisms. Thus the conductivity-temperature relationship for these thin films can be written as [28]:

$$\sigma(T) = \sigma_{01}\exp(-\Delta E_{\sigma 1}/k_B T) + \sigma_{02}\exp(-\Delta E_{\sigma 2}/k_B T) \quad (14)$$

where ΔE is the activation energy for conduction, σ_0 is the pre-exponential factor which depends on the compositions, k_B is Boltzmann constant, and T is the absolute temperature. The temperature at which the conduction mechanism seems to change is located at ~ 400 K (for x=10 and 20 %) and ~ 363 K (for x=30 %).

These temperatures are very close to the crystallization temperatures (T_c) of these films as obtained by the DTA. Thus the change in the dominant conduction mechanism with increasing temperature in our samples is thought to be due to the amorphous-crystalline transformation. Generally, such types of high and low temperature regions in CdSe thin films have been reported [29, 30].

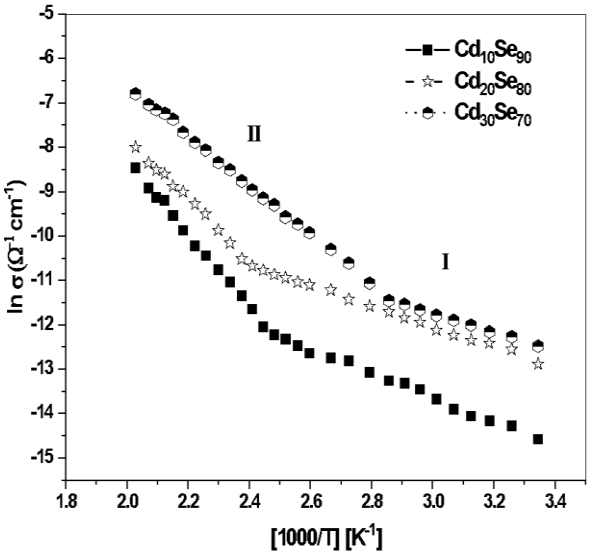

Fig. (6): plot of ln(σ) versus (10^3/T) for Cd_xSe_{100-x} (x=10, 20, 30 at. %) thin films

The activation energies $\Delta E_{\sigma 1}$ and $\Delta E_{\sigma 2}$ were calculated from the slope of the linear part of region (I) (300-370 K) and region (II) (370-500 K). While the intercepts on the y-axis gives the value of pre-exponential factors σ_{01} and σ_{02} for each conduction region. The room temperature conductivity σ_{RT}, the calculated activation energies and the pre-exponential factors are summarized in **Table 3**. In addition, values of the activation energies $\Delta E_{\sigma 1}$ and $\Delta E_{\sigma 2}$ are also plotted versus Cd content in **Fig. 7**. It is clear from **Table 3** that σ_{RT} increases, while $\Delta E_{\sigma 1}$, $\Delta E_{\sigma 2}$, σ_{01} and σ_{02} decreases as the Cd concentration increases. The decrease of the activation energies with increasing the Cd content can be ascribed to the decrease of the over all mean bond energy $\langle E \rangle$ for the studied samples as shown in Table 3. This decrease of $\Delta E_{\sigma 1}$, $\Delta E_{\sigma 2}$ can also be explained by the shift in Fermi level with increasing the Cd content. Amorphous chalcogenide semiconductors have characteristically charged defects (D^+, D^-) which pin the Fermi level near the middle of the energy gap of these semiconductors [31]. In the present system, Cd is assumed to form positively charged (D^+) defect centers due to the small electronegativity of Cd (1.69) as compared to Se (2.55). This excess creation of (D^+) defect centers can then unpin the Fermi level via increasing the number of tail states over the states near the Fermi level. These results are in good agreement with the previous work [32].

Table 3: Room temperature conductivity (σ_{RT}), activation energy (ΔE) and the pre-exponential factor (σ_0) for Cd_xSe_{100-x} (x=10, 20, 30 at. %) thin films.

Compositions	Room temperature conductivity σ_{RT} $(\Omega\ cm)^{-1}$	Activation Energy ΔE (eV)		Pre-exponential factor σ_0 $(\Omega\ cm)^{-1}$	
		$\Delta E_{\sigma 2}$	$\Delta E_{\sigma 1}$	σ_{02}	σ_{01}
$Cd_{10}Se_{90}$	4.69×10^{-7}	0.714	0.230	4.07×10^{3}	4.0×10^{-3}
$Cd_{20}Se_{80}$	2.55×10^{-6}	0.590	0.190	3.90×10^{2}	5.2×10^{-3}
$Cd_{30}Se_{70}$	3.81×10^{-6}	0.480	0.180	9.69×10^{1}	4.6×10^{-3}

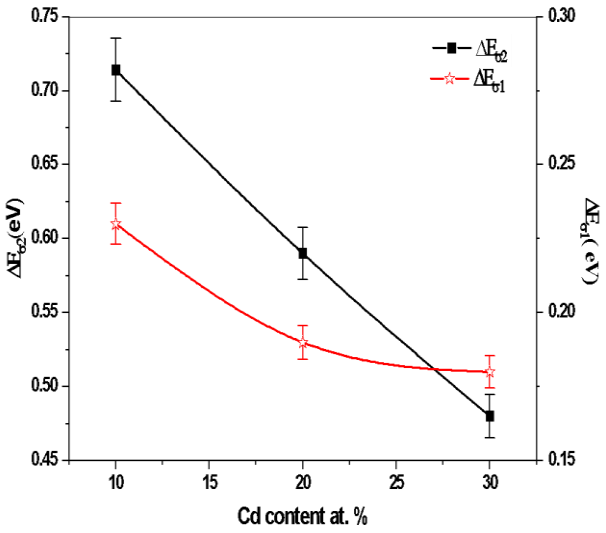

Fig. (7): Composition dependence of electrical activation energy ΔE_σ for Cd_xSe_{100-x} (x=10, 20, 30 at. %) thin films

To recognize the possible modes of conduction in our samples, the value of the pre-exponential factor σ_0 should be considered as it has been shown by Mott [33]. For the conduction in extended states, the value of the pre-exponential factor reported for a-Se and other Se alloyed films is of the order of 10^4 $(\Omega.cm)^{-1}$. A lower value for pre-exponential factor, 2 to 3 orders of magnitude, indicates the conduction in the localized states in the band tails [28, 34]. Even smaller values for σ_0 indicate conduction in the localized states near the Fermi level [35]. According to the values of the pre-exponential factor in Table 3, at lower temperatures (300 - 370 K), region (I), conduction occurs via variable range hopping of charge carriers in localized states near Fermi levels. But at higher temperatures (370 – 500 K), region (II), conduction in the extended states is dominant for all the studied compositions. It is also worthy to note that a decrease in the value of σ_{02} occurs with increasing the Cd content. Since the value of σ_{02} depends on the mobility of charge carriers and density of states, the observed variation may be due to the variation in these parameters with the material composition [36].

The observed variation in σ_{02} can be further understood in terms of its variation with $\Delta E_{\sigma 2}$, the so-called Meyer–Neldel rule (MNR) [37]. This rule is known to apply to various thermally activated phenomena. This rule correlates σ_{02} with $\Delta E_{\sigma 2}$ as:

$$\sigma_{02} = \sigma_{00} \exp(\Delta E_{\sigma 2} / k_B T_{MN}) \quad (15)$$

where σ_{00} and T_{MN} are constants, and $E_{MN} = k_B T_{MN}$ is known as the Meyer–Neldel characteristic energy. **Fig. 8** shows a plot of $\ln(\sigma_{02})$ versus $\Delta E_{\sigma 2}$, which can be best fitted to a straight line approving clearly that the dc conductivity of our thin films can be well described by the (MNR). The slope of the $\ln(\sigma_{02})$ versus $\Delta E_{\sigma 2}$ straight line yields the values of $E_{MN} \approx 62.3$ meV, which gives $T_{MN} = 722.9$ K for these chalcogenide alloys. The estimated values of E_{MN} and T_{MN} lies within the expected range of 25-100 meV and 260-950 K respectively, for the semiconductor materials [38, 39].

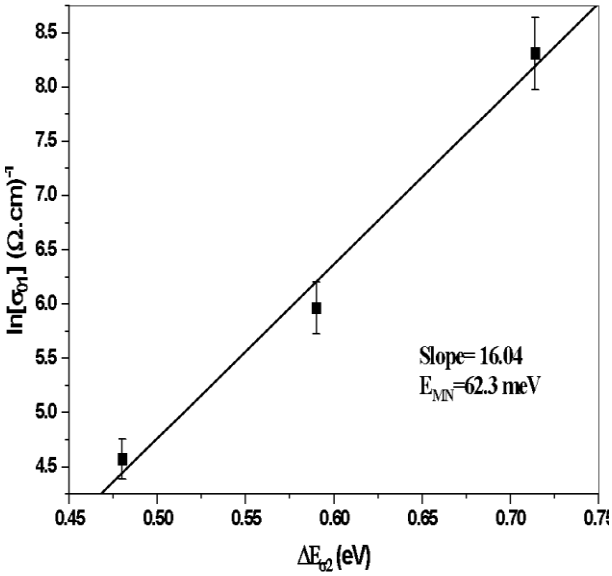

Fig. (8): Plot of $\ln(\sigma_{02})$ versus ΔE in the high temperature range for Cd_xSe_{100-x} (x=10, 20, 30 at. %) thin films

T_{MN} is the (MNR) characteristic temperature [34]. At this temperature, σ_{dc} is independent of activation energy ΔE. Different models have been applied for explaining Mayer-Neldel rule include the density of states (DOS) model, which is related to a systematic change in (DOS) in the mobility gap and statistical shift of Fermi energy E_F (T) [40]. **Fig. 9** represents a plot of $\ln(\sigma_{02})$ versus 1000/T for different thin films, with different activation energies. In such a plot, all curves should show one common intersection at T_{MN}. For studied films, the corresponding value for T_{MN} is determined to be 772 K, which is very close to the previously calculated value.

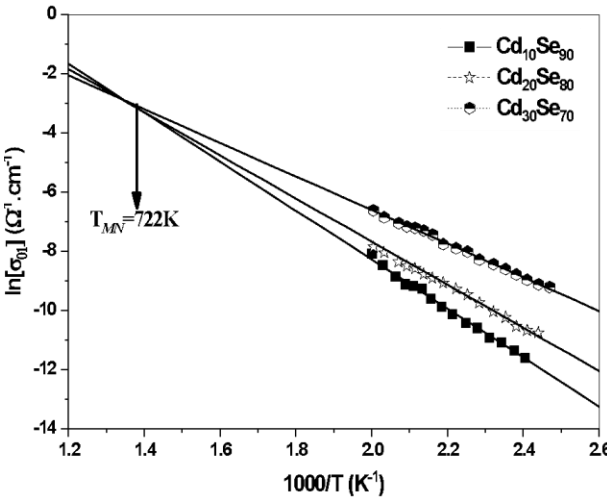

Fig. (9): Variation of extrapolated plot of ln(σ_{02}) versus 1000/T of Cd_xSe_{100-x} (x=10, 20, 30 at. %) thin films.

The conductivity data in the low-temperature region (T < 370K) are replotted in **Fig.10** according to Mott's relation for variable-range hopping (VRH) conduction [28]:

$$\sigma\sqrt{T} = \sigma_0^{\bullet} \exp\left[-A/T^{1/4}\right] \quad (16)$$

with

$$A^{1/4} = T_0 = 18\alpha^3/k_B N(E_F), \quad (17)$$

where α is the coefficient of exponential decay of the localized state wave function, which was assumed to be 0.124 $Å^{-1}$ [41], γ = 10^{13} Hz is the characteristic phonon frequency in most amorphous materials and $N(E_F)$ is the density of localized states at the Fermi level.

The obtained straight lines of Fig. (10) support our argument that the conduction at this temperature range may be due to hopping between localized states. Hence, the basic parameters characterizing VRH conduction, namely $N(E_F)$ and could be calculated from the slopes of these lines. Then, the values of the hopping distance R, hopping energy W and concentration of conduction electrons (n) within a range of K_BT of the Fermi energy were obtained by using the following relations [42, 43]:

$$R = \left[\frac{9}{8\pi\alpha k T N(E_F)}\right]^{1/4} \quad (cm) \quad (18)$$

$$W = \frac{3}{4\pi R^3 N(E_F)} = \left[\frac{2\alpha^3 k^3 T^3}{9\pi N(E_F)}\right]^{1/4} \quad (eV) \quad (19)$$

$$n = 2K_B T N(E_F) \quad (20)$$

The composition dependence of $\sigma_0^{\bullet}$, $N(E_F)$, n, R and W for the Cd_xSe_{100-x} (x=10, 20, 30 at.%) compositions are calculated and recorded in Table 4. It is noticed that T_0 decreases as the Cd content increase. Since T_o represents the degree of disorder, consequently the amorphicity of the samples decreases with increasing Cd content. Further, the pre-exponential factor $\sigma_0^{\bullet}$ decreases with increasing Cd content ensuring that the charge carrier mobility and density of states increases [44]. As shown in Table 4, W and αR are greater than kT and unity, respectively which satisfies the VRH model validity requirement [29].

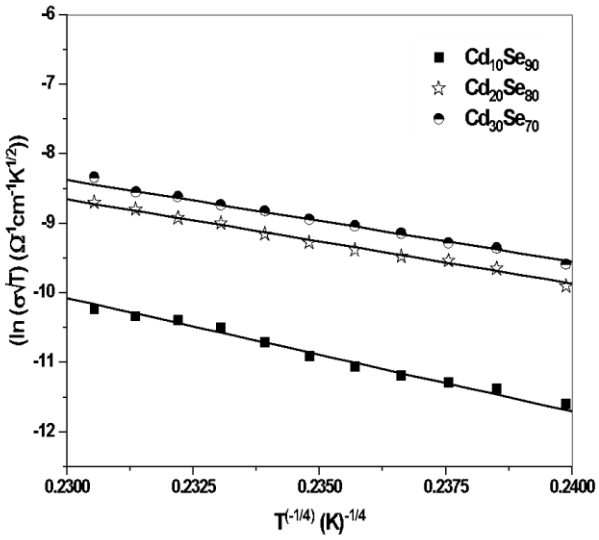

Fig. (10): Plots of ln ($\sigma T^{1/2}$) versus ($T^{-1/4}$) for Cd_xSe_{100-x} (x=10, 20, 30 at. %) thin films

Table 4: Mott's parameters for Cd_xSe_{100-x} (x=10, 20, 30 at. %) thin films.

Compositions	$\sigma_0^{\bullet}$ (Ω cm^{-1}K$^{1/2}$)	T_0 (K)	$N(E_F)$ ($eV^{-1}cm^{-3}$)	$n\times10^{16}$ (cm^{-3})	R (cm)	W (ev)	αR
$Cd_{10}Se_{90}$	3.78×10^{10}	5.06×10^{8}	7.87×10^{17}	4.069	1.09×10^{-6}	0.233	13.53
$Cd_{20}Se_{80}$	3.49×10^{8}	2.30×10^{8}	1.74×10^{18}	8.96	8.96×10^{-7}	0.191	11.11
$Cd_{30}Se_{70}$	1.92×10^{8}	2.03×10^{8}	1.96×10^{18}	10.16	8.68×10^{-7}	0.186	10.77

5. Conclusions

X-ray diffraction (XRD) results for as-prepared Cd_xSe_{100-x} (x=10, 20, and 30 at. %) thin films revealed an amorphous structure for these films except for $Cd_{30}Se_{70}$ where some Se crystallites were detected. These results were confirmed by SEM photographs and correlated to the rigidity percolation threshold (RPT) of the lattice. The d.c. conductivity for Cd_xSe_{100-x} (x=10, 20, and 30 at. %) thin films were measured in the temperature range

(300-500 K). The electrical transport of as-prepared Cd_xSe_{100-x} films is affected by two different mechanisms. In the high-temperature region (T > 370 K) the thermally activated conduction through the extended states takes place. The electrical activation energy (ΔE) and pre-exponential factor (σ_0) in this temperature range followed the well-known Meyer-Neldel rule (MNR). In the lower temperatures region (T < 370 K), the conductivity is dominated by the Mott's variable range hopping in the localized states near Fermi level. The density of states around Fermi level $N(E_F)$ and the concentration of conduction electrons (N) were calculated using Mott's parameters where it showed an increase with increasing of Cd content.

References

[1] A. Reisman, M. Berkenblit and M. Wizen, "Non-stoichiometry in cadmium selenide and equilibria in the system cadmium-selenium", J. Phys. Chem. 65(11) 2210-2214, 1962.

[2] C. D. Lokhande, R. V. Dabhade, P. S. Patil and S. H. Pawar, "Electrodeposition of CdSe and Cd(Se,Te) films and their performance in ECPV cells" Bulletin of Electrochemistry, 7, 319, 1991.

[3] D. Haneman, G. H. J. Wanternaar, R. C. Kainthala, "Improvements in lifetime of CdSe photoelectrochemical solar cells", Sol. Energy Mater. 10(1), 69-84, 1984.

[4] N. J. Kissinger, M. Jayachandran, K. Permual, S. Raja, "Structural and optical properties of electron beam evaporated CdSe thin films", B. Mater. Sci. 30, 547-551, 2007.

[5] S. Erat, H. Metin, M. Ari, "Influence of the annealing in nitrogen atmosphere on the XRD, EDX, SEM and electrical properties of chemical bath deposited CdSe thin films", Mater. Chem. Phys. 111(1), 114-120, 2008.

[6] D. Pathinettam Padiyan, A. Marikani, K. R. Murali, "Influence of thickness and substrate temperature on electrical and photoelectrical properties of vacuum-deposited CdSe thin films", Mater. Chem. Phys, 78(1), 51-58, 2003.

[7] S. Velumani, Xavier Mathew, P. J. Sebastain, Sa. K. Narayandass, D. Mangalaraj, "Structural and optical properties ofhot wall deposited CdSe thin films", Sol. Energy Mater. Sol. Cells 76, 347-358, 2003.

[8] S. K. Kaushish, T. P. Sharma, "Study of optical constants in CdxSe1−x" Optical Materials, 14(4), 297-301, 2000.

[9] A. I. Khudiar, M. Zulfequar, Z. H. Khan, "Influence of cadmium concentration on the optical and structural properties of cadmium selenide thin films", Mat. Sci. Semicon. Proc. 15(5) 536-542, 2012.

[10] H. Mahfoz Kotb, M.A. Dabban, F.M. Abdel-Rahim, A.Y. Abdel-latif, M.M. Hafiz, "Thermally induced effects on structural and electrical properties of selenium-rich Cd-Se thin films" Physica B, 406 (6-7),1326-1329, 2011.

[11] H. Mahfoz Kotb, M.A. Dabban, A.Y. Abdel-latif, M.M. Hafiz," Annealing Temperature Dependence of the optical and Structural Properties of Selenium-Rich Cd-Se Thin Films" J. Alloy. Comp, 512(1), 115-120, 2012.

[12] J. C. Phillips, "Ionicity of the Chemical Bond in Crystals", Rev. Mod. Phys. 49, 317, 1970.

[13] A. Dahshan, "Optical and other physical characteristics of Ge–Se–Cd thin films", Opt. Mater. 32(1), 247-250, 2009.

[14] P. K. P. Kalita, B. K. Sarma, H. L. Das, "Structural characterization of vacuum evaporated ZnSe thin films", B. Mater. Sci. 23(4), 313-317, 2000.

[15] L. Pauling. The Nature of the Chemical Bond, 3rd Ed., Cornell Univ. Press, New York, p180, 1960.

[16] William M. Haynes, CRC Handbook of Chemistry & Physics, 91st Edition, CRC Press, 2010.

[17] L. Tichy, H. Ticha, "Covalent bond approach to the glass-transition temperature of chalcogenide glasses", J. Non-Cryst. Solids. 189(1-2) 141-146, 1995.

[18] R. Sathyamoorthy, J. Dheepa, "Structural characterization of thermally evaporated Bi2Te3 thin films", J. Phys. Chem. Sloids. 68(1)111-117, 2007.

[19] M. F. Thrope, "Continuous deformations in random networks", J. Non-Cryst. Solids, 57(3), 355-370, 1983.

[20] K.,Vitalij. Pecharsky, Fundamentals of powder diffraction and structural characterization of materials, Springer, 2005.

[21] U Pal, D. Samanta, S. Ghorai, B. K. Samantaray, A. K. Chaudhuri, "Structural characterization of cadmium selenide thin films by X-ray diffraction and electron microscopy", J. Phy. D: Appl. Phys. 25 1488, 1992.

[22] A. J. P. Wilson, Mathematical Theory of X-ray Powder Diffractometry, Gordon and Breach, New York, 1963.

[23] S. B. Qadri, E. F. Skelton, D. Hsu, A. D. Dinsmore, J. Yang, H. F. Gray, B. R. Ratna, "Size-induced transition-temperature reduction in nanoparticles of ZnS", Phys. Rev. B, 60, 9191, 1999.

[24] S. Venkatachalam, D. Mangalaraj, Sa. K. Narayandass, "Characterization of vacuum-evaporated ZnSe thin films" Physica B 393(1-2), 47-55, 2007.

[25] G. B. Williamson, R. C. Smallman, "III. Dislocation densities in some annealed and cold-worked metals from measurements on the X-ray debye-scherrer spectrum" Phil. Mag. 1(1), 34-46, 1956.

[26] J. C. Phillips and M. F. Thorpe, "Constraint theory, vector percolation and glass formation", J. Solid State Commun., 53:699-702, 1985.

[27] S.A. Fayek, A.F. Maged, M.R.Balboul, "Optical and electrical properties of vacuum evaporated In doped Se amorphous thin films", Vacuum 53(3-4), 447-450, 1999.

[28] N. F. Mott, E. A. Davis, Electronic Processes in Non-Crystalline Materials, 2nd Ed. Clarendon, Oxford, 1979.

[29] R. B. Kale, C.D. Lokhande, "Influence of air annealing on the structural, optical and electrical properties of chemically deposited CdSe nano-crystallites", Appl. Surf. Sci. 223(4), 343-351, 2004.

[30] R. Lozada-Morales,a M. Rubín-Falfán,a O. Portillo-Moreno,b J. Pérez-Álvarez,b R. Hoyos-Cabrera,b C. Avelino-Flores,b O. Zelaya-Angel,c O. Guzmán-Mandujano,d P. del Angel,d J. L. Martínez-Montes,e and L. Baños-López, "Properties of CdSe Polycrystalline Thin Films Grown by Chemical Bath", J. Electrochem. Soc. 146 (7), 2546, 1999.

[31] N. Toghe, T. Minami, Y. Yamamoto, M. Tanaka, "Electrical and optical properties of n-type semiconducting chalcogenide glasses in the system Ge-Bi-Se", J. Appl. Phys.51, 1048-1053, 1980.

[32] S. A. Fayek, S.M.El Sayed, "Effect of composition and forming parameter on evaporated CdSeTe films deposited at room temperature" J. Phys. Chem. Solids 63(1), 1-8, 2002.

[33] N. F. Mott, "Conduction in non-Crystalline systems: IV. Anderson localization in a disordered lattice" The Philosophical Magazine: A Journal of Theoretical Experimental and Applied Physics, 22(175), 7-29. 1970.

[34] E. A. Davis, N. F. Mott, "Conduction in non-crystalline systems V. Conductivity, optical absorption and photoconductivity in amorphous semiconductors", Philos. Mag. 22 (179), 903-922, 1970.

[35] M. A. Majeed Khan, M. Zulfequar, M. Husain, "Estimation of the density of localized states of a-Se100−xBix films from electrical properties", Physica B, 322, 1-11, 2002.

[36] V. Pamukchieva, Z. Levi, E. Savova, "DC electrical conductivity in glasses and thin films" Semicond. Sci. Technol. 13(11), 1309, 1998.

[37] R. Metselaar, G. Oversluizen, "The meyer-neldel rule in semiconductors", Journal of Solid State Chemistry 55(3), 320-326, 1984.

[38] V. Kirbs, t. Druesedau, H. Fiedler, "Thermally induced metastability and the Meyer-Neldel rule in hydrogenated amorphous silicon", J. Phys.: Condens. Mat., 2 (36), 7473, 1990.

[39] F. Abdel-Wahab, "Signature of the Meyer–Neldel rule on the correlated barrier-hopping model", J. Appl. Phys., 91(1) 265-270, 2002.

[40] K. Morii, T. Matsui, H. Tsuda, H. Mabuchi, "Meyer–Neldel rule in amorphous strontium titanate thin films" Appl. Phys. Lett., 77, 2361-2363, 2000.

[41] S. Mahadevon, A. Giridhar, K. J. Ron, "Study of electron transport in As-Se-Te glasses", J. Phys. C 10:2, 4499, 1977.

[42] R. M. Hil, "Hopping conduction in amorphous solids", Philos. Mag. 24 1307-1325, 1971.

[43] P. Nagels, L. Tichý, H. Tichá, J. "Observation of variable-range hopping conduction in a Ge-Sb-S glass alloyed with CoS", Non-Cryst. Solids. 164 (2), 1187-1190, 1993.

[44] M. M. Abd El-Raheem, "Electrical properties of GeSeTl thin films deposited by e-beam evaporation technique", Mater. Chem. Phys. 116, 353-357, 2009.

مقالة بحثية

الخصائص التركيبية والكهربائية لأغشية الكادميوم-سيلينيد الرقيقة غير المتكافئة

عبدالله عمر علي[1،*]، مهدي احمد دبان[1]، هشام الدين محفوظ قطب[2]

[1] قسم الفيزياء، كلية العلوم، جامعة عدن، عدن، ص.ب. 6312،اليمن
[2] قسم الفيزياء، كلية العلوم، جامعة أسيوط، مصر

* الباحث الممثّل: عبدالله عمر علي؛ البريد الالكتروني: abdullah.omer.scie@aden-univ.net

استلم في: 02 أغسطس 2023 / قبل في: 16 أغسطس 2023 / نشر في 30 سبتمبر 2023

المُلخّص

تم تحضير سبائك غير متكافئة Cd_xSe_{100-x} (x = 10, 20 and 30 at. %) بتقنية الصهر-التبريد المفاجئ، بينما تم تحضير الأغشية الرقيقة لهذه السبائك بتقنية التبخير الحراري الفراغي. أظهرت نتائج التحليل الحراري التفاضلي أن التركيب يؤثر على درجات الحرارة المميزة، على سبيل المثال، التحول الزجاجي، ودرجات حرارة التبلور. أكدت أنماط حيود الأشعة السينية للأغشية الرقيقة البكر للسبائك أنها في حالة أمورفية ماعدا تلك التي تحتوي على نسبة 30% من الكادميوم فقد ظهرت في الحالة شبة الأمورفية حيث وجدت قمة وحيدة لحيود الأشعة السينية. هذه النتائج توافقت مع ما أظهرته صور الميكروسكوب الالكتروني الماسح لتلك الأغشية وربطها بعتبة ترشيح الصلابة للشبكة. من ناحية أخرى أوضحت أنماط حيود الأشعة السينية عمليات التحول من التركيب الامورفي إلى المتبلور بعد المعالجة الحرارية للأغشية الرقيقة للسبائك في المدى من درجات حرارة (423 كلفن) لمدة نصف ساعة. كما تم حساب المعاملات التركيبية مثل الحجم البلوري والانفعال وكثافة الانخلاعات لكلا الطورين السلينيوم والكادميوم-سيلينيد. دُرست الموصلية الكهربية للأغشية مع تغير درجة الحرارة في المدى من (300-500 كلفن) كدالة في محتوى الكادميوم. ومن القياسات الكهربية وجد ان لهذه الأغشية طاقتي تنشيط مختلفتين (سلوكين مختلفين) أحدهما في يتم في المستويات الممتدة في مدى درجات الحرارة المرتفعة (370-500 كلفن) والأخرى في مدى درجات الحرارة المنخفضة (300-370 كلفن) عن طريق قفز حوامل الشحنة في المستويات الموضعية قرب مستوى فيرمي. كما لوحظ أن سلوك العينات في مدى درجات الحرارة المرتفعة يتبع قاعدة ماير-نيلدل.

الكلمات المفتاحية: سيلينيد الكادميوم، الأغشية الرقيقة، عتبة ترشيح الصلابة، الموصلية المستمرة، قاعدة ماير-نيلدل.

How to cite this article:

A. O. Ali, M. A. Dabban, and H. M. Kotb, “THE STRUCTURAL AND ELECTRICAL PROPERTIES OF NON-STOICHIOMETRIC CADMIUM SELENIDE THIN FILMS”, *Electron. J. Univ. Aden Basic Appl. Sci.*, vol. 4, no. 3, pp. 237-248, September. 2023. DOI: https://doi.org/10.47372/ejua-ba.2023.3.273